Cerebral Circulation - Cognition and Behavior 4 (2023) 100162

Contents lists available at ScienceDirect

Cerebral Circulation - Cognition and Behavior

journal homepage: www.sciencedirect.com/journal/cerebral-circulation-cognition-and-behavior

Impaired oxygen extraction and adaptation of intracellular energy metabolism in cerebral small vessel disease

Annemarie Reiländer [a,b,1], Ulrich Pilatus [c,1], Jan-Rüdiger Schüre [c], Manoj Shrestha [b], Ralf Deichmann [b], Ulrike Nöth [b], Elke Hattingen [c], René-Maxime Gracien [a,b], Marlies Wagner [b,c], Alexander Seiler [a,b,*]

[a] Department of Neurology, Goethe University Hospital Frankfurt, Schleusenweg 2-16, Frankfurt 60528, Germany
[b] Brain Imaging Center, Goethe University Hospital Frankfurt, Frankfurt Germany
[c] Institute of Neuroradiology, Goethe University Hospital Frankfurt, Frankfurt Germany

ARTICLE INFO

Keywords:
Small vessel disease
Oxygen extraction fraction
Cellular energy metabolism
MR spectroscopy
quantitative MRI
Microstructural impairment

ABSTRACT

Background: We aimed to investigate whether combined phosphorous (^{31}P) magnetic resonance spectroscopic imaging (MRSI) and quantitative T_2' mapping are able to detect alterations of the cerebral oxygen extraction fraction (OEF) and intracellular pH (pH_i) as markers the of cellular energy metabolism in cerebral small vessel disease (SVD).

Materials and methods: 32 patients with SVD and 17 age-matched healthy control subjects were examined with 3-dimensional ^{31}P MRSI and oxygenation-sensitive quantitative T_2' mapping ($1/T_2' = 1/T_2^* - 1/T_2$) at 3 Tesla (T). PH_i was measured within the white matter hyperintensities (WMH) in SVD patients. Quantitative T_2' values were averaged across the entire white matter (WM). Furthermore, T_2' values were extracted from normal-appearing WM (NAWM) and the WMH and compared between patients and controls.

Results: Quantitative T_2' values were significantly increased across the entire WM and in the NAWM in patients compared to control subjects (149.51 ± 16.94 vs. 138.19 ± 12.66 ms and 147.45 ± 18.14 vs. 137.99 ± 12.19 ms, $p < 0.05$). WM T_2' values correlated significantly with the WMH load (ρ=0.441, $p = 0.006$). Increased T_2' was significantly associated with more alkaline pH_i (ρ=0.299, $p < 0.05$). Both T_2' and pH_i were significantly positively correlated with vascular pulsatility in the distal carotid arteries (ρ=0.596, $p = 0.001$ and ρ=0.452, $p = 0.016$).

Conclusions: This exploratory study found evidence of impaired cerebral OEF in SVD, which is associated with intracellular alkalosis as an adaptive mechanism. The employed techniques provide new insights into the pathophysiology of SVD with regard to disease-related consequences on the cellular metabolic state.

1. Introduction

Cerebral small vessel disease (SVD) is one of the most frequent etiologies of ischemic stroke and a leading cause of cognitive impairment in the elderly [1–4]. Apart from being increasingly prevalent in higher age groups, SVD is strongly associated with arterial hypertension and diabetes as the most common risk factors [1]. The pathological processes leading to progressive damage of the cerebral vasculature with resulting detrimental effects on the supplied brain parenchyma are mainly characterized by lipohyalinosis and fibrinoid necrosis and affect the smaller perforating arteries and arterioles, but also capillaries and veins [1,5]. Neuroimaging correlates of SVD include - among others - white matter hyperintensities (WMH) as the predominant manifestation, as well as lacunar infarcts and cerebral microbleeds (CMB) [1]. WMH are typically

Abbreviations: MRS, magnetic resonance spectroscopy; MRSI, magnetic resonance spectroscopic imaging; MRI, magnetic resonance imaging; SVD, cerebral small vessel disease; OEF, oxygen extraction fraction; pH_i, intracellular pH; WM, white matter; NAWM, normal-appearing white matter; WMH, white matter hyperintensities; CBF, cerebral blood flow; CBV, cerebral blood volume; $CMRO_2$, Cerebral metabolic rate of oxygen; BBB, blood-brain barrier; Hb, hemoglobin; DTI, diffusion tensor imaging; PI, Pulsatility index; ICA, internal carotid artery; RF, radio frequency; GE, gradient echo; TR, repetition time.

* Corresponding author at: Department of Neurology, Goethe University Hospital Frankfurt, Schleusenweg 2-16, Frankfurt 60528, Germany.
E-mail address: Alexander.Seiler@kgu.de (A. Seiler).

[1] These authors contributed equally to this work.

https://doi.org/10.1016/j.cccb.2023.100162
Received 14 November 2022; Received in revised form 25 January 2023; Accepted 9 February 2023
Available online 10 February 2023

located in the periventricular and deep white matter of the cerebral hemispheres and appear hyperintense in T2-weighted and fluid-attenuated inversion recovery (FLAIR) sequences [1]. They are the result of myelin loss and gliosis due to arteriolar occlusion with subsequent ischemia and typically exhibit reduced cerebral blood flow (CBF) and cerebral blood volume (CBV) [5–9]. Apart from the WMH, also the surrounding normal-appearing white matter (NAWM) and crossing fibers intersected by the white matter lesions show impaired perfusion in patients with SVD [9–11]. This finding indicates a widespread vascular dysfunction, which involves larger parts of the cerebral white matter and goes beyond the visible WMH [9,12].

In cerebral large-artery steno-occlusive disease, impaired perfusion leads to an increase of the cerebral oxygen extraction fraction (OEF) in order to maintain a constant cerebral metabolic rate of oxygen ($CMRO_2$) when the vascular autoregulatory capacity is exhausted [13–16]. In contrast, SVD can be associated with a reduction of the tissue oxygen tension and the oxygen extraction capacity, leading to an overall decrease of the OEF and the cellular oxygen consumption [9,17]. Pathophysiologically, microcirculatory disturbances with unfavorable heterogeneous capillary blood flow patterns impeding the maximal augmentation of the cerebral OEF play a relevant role for the compromise of oxygen metabolism in SVD [9,17,18]. Furthermore, also the oxygen diffusivity at the exchange level of the capillary bed can be decreased due to thickening of the capillary wall as well as enlargement of the extracellular space as a consequence of blood-brain barrier (BBB) leakage and subsequent interstitial edema [5,19–21]. It is plausible to assume that in an attempt to preserve their structural integrity under the condition of restricted oxygen supply in SVD, neuronal cells are constrained to adjust their intracellular energy metabolism. Consequently, within the limits of the cellular compensatory capacity, long-term adaptation processes of the cellular energy metabolism might enable to meet the basal metabolic needs at reduced oxygen supply.

Those presumed changes of intracellular energy metabolism have not yet been investigated along with surrogate markers of cerebral oxygen metabolism in patients with SVD. Phosphorus (^{31}P) MR spectroscopy (MRS) provides biochemical information on the tissue metabolic state [22]. Besides the assessment of various metabolite concentrations, such as markers of membrane and energy metabolism, it allows for measuring the intracellular pH (pH_i) [22,23]. Under ischemic conditions such as chronic cerebral hypoperfusion and subacute stroke, a shift in pH_i towards alkaline values has been reported [23–26]. Furthermore, pH_i showed a negative correlation with the relaxation time T_2' in those patients, pointing towards an association between reduced oxygen supply and more alkaline pH_i values [27]. These alkaline pH_i changes may reflect slow adaptation processes of cerebral energy metabolism in response to reduced blood and oxygen supply, including an increased glycolysis rate to compensate for impaired oxidative phosphorylation [28]. In this exploratory and pathophysiological study, we aimed to investigate changes of intracellular energy metabolism and tissue oxygenation in SVD in order to gain deeper insights into the disease-related alterations of the cellular metabolic state as a potential surrogate marker of disease severity, which goes beyond measurable impairment of the tissue microstructure. For this purpose, ^{31}P MRS was combined with quantitative T_2' ("T_2 prime") mapping. T_2' is obtained from a correction of the effective transverse relaxation time T_2* for spin-spin (T_2) effects and is calculated by applying the formula: $1/T_2' = 1/T_2^* - 1/T_2$. Due to the correction for spin-spin effects, T_2' in comparison to T_2* shows an increased sensitivity to local changes of the ratio between oxygenated hemoglobin (Hb), which is diamagnetic, and deoxygenated Hb, which is paramagnetic, irrespective of signal alterations caused by e.g. tissue edema or gliosis. Therefore, T_2' maps provide information on the extent of blood oxygenation and T_2' represents an established surrogate marker of the cerebral OEF [29–33]. We hypothesized that quantitative T_2' mapping might be able to detect a potential reduction of the OEF in SVD and that T_2' and pH_i are complementary imaging parameters and might represent interrelated aspects of essential cellular metabolic processes. In order to confirm a relevant disease stage of SVD, both from a clinical and a microstructural point of view, additional comprehensive cognitive testing and diffusion tensor imaging (DTI) were performed.

2. Material and methods

2.1. Subjects

Between January 2017 and June 2019, 32 patients with sporadic SVD and 17 age-matched healthy control subjects were included in this study. Patients were recruited from the Department of Neurology at the Goethe University Hospital Frankfurt, Germany. SVD was defined as the presence of confluent WMH on conventional MRI (corresponding to Fazekas grade ≥ 2). The patients were mainly referred to the hospital for lacunar stroke or transient ischemic attack, chronic SVD-related symptoms (such as cognitive decline or gait impairment), or other neurological conditions with WMH as an incidental finding in conventional MRI. Exclusion criteria were cognitive impairment or dementia with suspected neurodegenerative origin, relevant stenosis of a brain-supplying artery (degree of $\geq$50%), non-lacunar stroke, white matter lesions not compatible with sporadic SVD (e.g. inflammatory origin) and common MRI contraindications. Control subjects were recruited mainly through public advertising. Additional control subjects were recruited from the neurological department whose diagnostic workup had not revealed any neurological disorder. Inclusion criteria for control subjects were a medical history without neurological or psychiatric disease and common vascular risk factors (apart from controlled arterial hypertension), and the absence of confluent white matter hyperintensities on T2-weighted/ FLAIR imaging (Fazekas grade ≤ 1). Healthy subjects with MRI contraindications were excluded as well. The subjects included in this study partly overlap with a previously described cohort [34]. The study was approved by the institutional review board of the medical faculty of the Goethe University, Frankfurt and conducted in accordance with the Helsinki Declaration (revised version from 1983). Written informed consent was obtained from each subject before enrolment in the study.

2.2. MR imaging protocol

MRI data acquisition was performed on two 3T whole body scanners (Magnetom Trio and Prisma, Siemens Medical AG, Erlangen, Germany), equipped with a body coil for radio-frequency (RF) transmission and an 8 (Trio) or 20 (Prisma) channel phased-array head coil for RF reception. For ^{31}P MRS measurements, a double-tuned $^{1}H/^{31}P$ volume head coil (Rapid Biomedical, Rimpar, Germany) was used.

2.2.1. MR spectroscopic imaging

The ^{31}P MRSI data were acquired recording the free induction decay (FID) after a 60° excitation pulse, using a 3D circular weighted phase encoding scheme with TR/TE = 2000 ms/ 2.3 ms, FoV 240 × 240 × 200 mm^3, matrix = 8 × 8 × 8 mm^3, extrapolated to 16 × 16 × 16 mm^3, nominal voxel size after interpolation = 15 × 15 × 12.5 mm^3, WALTZ4 ^{1}H decoupling, number of averages (NA) of 10 at the center of k-space, bandwidth = 2000 Hz, scan time = 10:44 min. As a reference image for the further analysis of the MRSI data, a T2-weigthed (T2w) turbo spin echo sequence was performed with TR/TE= 3300/102 ms, FoV 240 × 191 mm^2, matrix size = 256 × 163, voxel size = 0.94 × 1.17 mm^2, 20 axial slices, slice thickness = 5 mm, inter-slice gap 1 mm, refocusing angle 150°, bandwidth = 100 Hz/Px, scan time = 1:08 min.

2.2.2. Quantitative T_2 and T_2* mapping with motion correction

T_2 mapping was based on a fast spin-echo sequence with an echo-

train length of 11 echoes per excitation, an echo spacing of 17.1 ms, and the following imaging parameters: 25 axial slices (2 mm thickness, 1 mm interslice gap), TR = 5000 ms, BW = 100 Hz/pixel, 180° refocusing pulses, FOV = 240 × 180 mm^2, matrix size = 192 × 144 (readout × phase encoding), in-plane resolution = 1.25 × 1.25 mm^2. For quantitative T_2 mapping, 5 datasets were acquired with different TE values (17, 86, 103, 120, 188 ms), keeping all other acquisition parameters constant. The total duration was 6:25 min.

Mapping of T_2* was based on the acquisition of eight multiple-echo gradient echo (GE) datasets with export of phase and modulus data: FOV = 240 × 180 mm^2, matrix size = 192 × 144 (readout × phase encoding), in-plane resolution = 1.25 × 1.25 mm^2, 25 axial slices, slice thickness = 2 mm, inter-slice gap = 1 mm, TE = [10,16,22,28,34,40,46,52] ms, TR = 1500 ms, excitation angle (α) = 30°, BW = 299 Hz/Pixel, duration = 3:36 min.

For motion correction, the acquisition was repeated twice with reduced spatial resolution (and therefore reduced k-space coverage) in phase encoding direction, covering only the central 50% (duration = 1:57 min) and 25% (duration = 1:03 min) of k-space.

2.2.3. Diffusion tensor imaging and structural imaging

DTI as well as structural imaging (T1-weighted Magnetization-Prepared Rapid Acquisition of Gradient Echos (MP-RAGE), FLAIR) data were acquired as explained previously in detail [34].

2.3. Image post-processing and analysis

2.3.1. Post-processing and analysis of MRSI data

^{31}P MRS data were registered to 2D-anatomical data using an in-house developed software tool written in MatLab (MathWorks, Natick, MA, USA). A graphical user interface included in this tool enabled the selection of voxels from the 3D spectroscopic data set using T2-weighted reference images with a MRS grid overlay. In general, ^{31}P MRS allows the analysis of spectra in a representative volume-of-interest (minimum size of voxel after extrapolation 15 × 15 × 12.5 mm^3). Therefore, in order to reduce partial volume effects from less affected tissue, if necessary the grid was shifted to place at least one voxel per hemisphere in tissue with WMH (usually at the level of the lateral ventricles above the basal ganglia) in the patients' datasets (Fig. 1A). Subsequently, the voxel with the highest load of WMH in each hemisphere was selected for further analysis. In the data sets of control subjects we identified voxels in deep white matter anatomically corresponding to the selected voxels of the patients' data (Fig. 1B). Here, the grid was also shifted as needed to avoid inclusion of cerebrospinal fluid or gray matter in the selected voxels as best as possible. For each selected voxel, the ^{31}P MRSI data were analyzed in the time domain with a nonlinear least-square fitting algorithm (AMARES) implemented in the program jMRUI (http://www.mrui.uab.es, version 4.0) [35]. The fit was restricted to the metabolites adenosine-triphosphate (ATP), inorganic phosphate (Pi), phosphocreatine (PCr), phosphoethanolamine (PEth), glycerophosphoethanolamine (GPE), phosphocholine (PCho) and glycerophosphorylcholine (GPC) (Fig. 1). pH_i was calculated from the chemical shift difference between the metabolites Pi and PCr using the formula pH = pkA + 10log ([δ1–δ0]/[δ0–δ2]) as implemented in jMRUI (default values: pkA = 6.75 ppm, δ1 = 3.27 ppm, δ2 = 5.63 ppm) [36]. Further to pH_i evaluation, we used the ratios PCr/Pi and ATP/Pi for further analyses as surrogate markers of the cells' ability to control their energy production [37]. Higher ratios are indicative of higher (relative) energy-rich substrate concentrations as compared to concentrations of low-energy metabolites.

2.3.2. Post-processing of quantitative T_2 and T_2* maps for calculation of T_2'

All further imaging data were processed with MatLab as well as shell scripts utilizing tools from the FMRIB's Software Library (FSL, version 5.0.7) and SPM 12 (Wellcome Department of Cognitive Neurology, UCL Institute of Neurology, London, United Kingdom). Skull-stripping of the imaging data (apart from MRSI postprocessing, which is described under 2.3.1) was performed with 'BET' [38]. T_2- and T_2*-mapping was performed via mono-exponential fitting of the signal in the series of FSE (T2) or GE (T2*) data sets obtained with multiple TE. T_2* mapping included an algorithm for subject motion correction, replacing motion-affected lines in k-space by the respective lines acquired in the additional data sets with reduced k-space sampling [39]. Signal losses induced by B0 distortions were corrected for in the T2*-weighted data before exponential fitting. T_2* maps were co-registered to the T_2 maps (six degrees of freedom). T_2' maps were derived from T_2* and T_2 maps according to the formula: $1/T_2' = 1/T_2^* - 1/T_2$.

2.3.3. Post-processing of DTI data

DTI data were postprocessed as reported previously in detail [34] to calculate parametric maps of the fractional anisotropy (FA) and mean diffusivity (MD) as established parameters of the white matter (WM) microstructural tissue integrity in SVD [40,41].

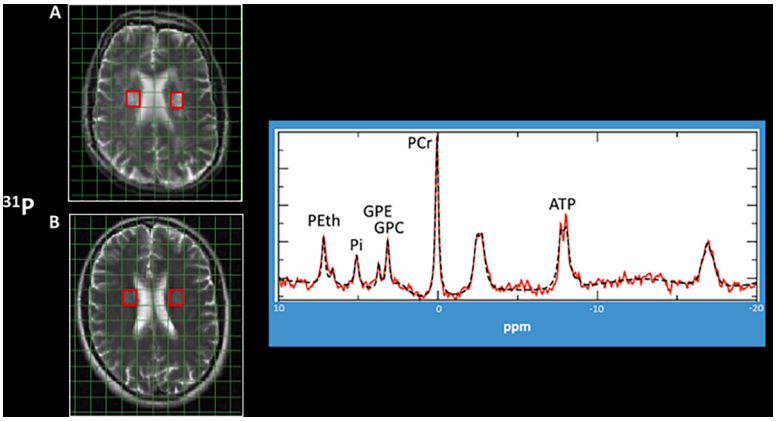

Fig. 1. Illustration of voxel selection for ^{31}P magnetic resonance spectroscopic (MRS) analysis in a SVD patient (A) and a healthy control subject (B) in a slice at the level of the lateral ventricles above the basal ganglia level. One exemplary spectrum is shown on the right. GPC: glycerophosphocholine; GPE: glycerophosphoethanolamine; PCr: phosphocreatine; ATP: adenosine-triphosphate; PEth: phosphoethanolamine; Pi: inorganic phosphate.

2.3.3. Post-processing of structural imaging data: tissue segmentation for quantitative analyses and assessment of conventional SVD imaging markers

WMH were automatically segmented on skull-stripped FLAIR images (Fig. 2A). In brief, a custom-built MATLAB script employing functions from the MRIcron software (Chris Rorden, Columbia, SC, USA; www.mricro.com) was used to segment the WMH based on FLAIR signal intensities and histogram analyses as described earlier in detail [34]. If necessary, the WMH segmentations were corrected manually by two experienced neurological/neuroradiological readers, who also evaluated the number of lacunes and CMBs in each subject. During this procedure, standardized consensus criteria [42] were applied for the identification and assignment of the respective lesions based on the FLAIR, T1- and T2*-weighted images. Based on the evaluated and corrected individual WMH segmentation (Fig. 2B, red areas), the total WMH volume was calculated for each subject.

Tissue segmentation of the T1-weighted MP-RAGE datasets was performed with SPM 12, thresholding the WM tissue probability map at 70% to obtain a binary WM mask. For quantitative image analyzes, FLAIR and T1-weighted images were linearly co-registered ('FLIRT', FSL) to the target data set created for T_2 mapping [43]. The resulting co-registration matrices were applied to the WMH mask and WM mask for co-registration to the target data set. A mask of the NAWM (Fig. 2B, light blue region) was generated by eliminating voxels inside the WMH mask from the WM mask. In order to perform image analyses in a common image space, FA and MD maps were linearly co-registered to the target data set created for T_2 mapping. For minimization of partial volume effects, cerebrospinal fluid (CSF) compartments were removed from the parameter maps by excluding voxels inside a CSF mask obtained from tissue segmentation. The individual WM and WMH masks were used to read mean T_2' (Fig. 2C), FA and MD values across WM, WMH and NAWM from the respective parameter maps.

The normalized brain volume (NBV), which represents the brain volume relative to the individual skull size, thus being a volume measure sensitive to atrophy, was obtained from the MP-RAGE datasets using the FSL tool 'SIENAX' [44,45], which was also used to determine the total intracranial volume (ICV).

2.4. Carotid doppler/ultrasound examination

Doppler/ultrasound of the distal internal carotid arteries (ICA) was performed using a Philips Affinity 70 G ultrasound machine, equipped with a 2 MHz ultrasound probe. Vascular pulsatility was measured in a systematic manner on a transversal section below the skull base. The Pulsatility Index (PI, Gosling Index) was calculated automatically with the device's software applying the formula: PI = (peak systolic flow velocity - minimal systolic flow velocity) / mean flow velocity. For further analyses, the PI was averaged between both sides to obtain the ICA-PI.

2.5. Cognitive assessment

Cognitive performance was assessed using the German version of the Consortium to Establish a Registry for Alzheimer's Disease - Neuropsychological Assessment Battery (CERAD-NAB, CERAD-plus version) including three tests of the 'subcortical' cognitive domains executive functioning und mental speed (Trail Making Test (TMT) part A and B, S-Words) [46,47]. To correct for the influence of demographic variables, raw scores of the CERAD-plus test battery were converted to standardized z-scores adjusted for age, sex and education, based on two normative samples for the German CERAD-plus version and by the means of a freely available Excel® application (https://www.memoryclinic.ch) [47,48]. Since TMT-A, TMT-B and 'S-words' as markers of executive functioning are of particular relevance in cerebral small vessel disease, these tests were evaluated separately [49,50]. Furthermore, an executive function composite score was calculated by averaging the z-scores of these tests. As a global measure of cognitive performance, a composite score similar to the Chandler CERAD total score was calculated by averaging the z-Scores of six CERAD-NAB variables (verbal fluency, Boston Naming Test, word list learning, word list recall, word list recognition and constructional praxis) [51].

2.6. Statistical analysis

A chi-square test was used to compare categorical variables between the groups. Other demographic characteristics as well as the imaging parameters were tested for normal distribution with the Kolmogorov-Smirnov-test. Due to the skewed distribution, WMH volumes were normalized to the individual ICV for further statistical analyses. For group comparisons of not normally distributed variables the Mann-Whitney-*U* test was applied. Normally distributed parameters were compared with unpaired t-tests after evaluation for homogeneity of variance using the Levene-test. Pearson's correlation (for normally distributed parameters), respectively Spearmańs rank correlation (for not normally distributed parameters) were applied to test for significant parameter correlations. Statistical analyses were performed with IBM SPSS 27 (Armonk, NY). All tests were two-sided and a $p < 0.05$ was

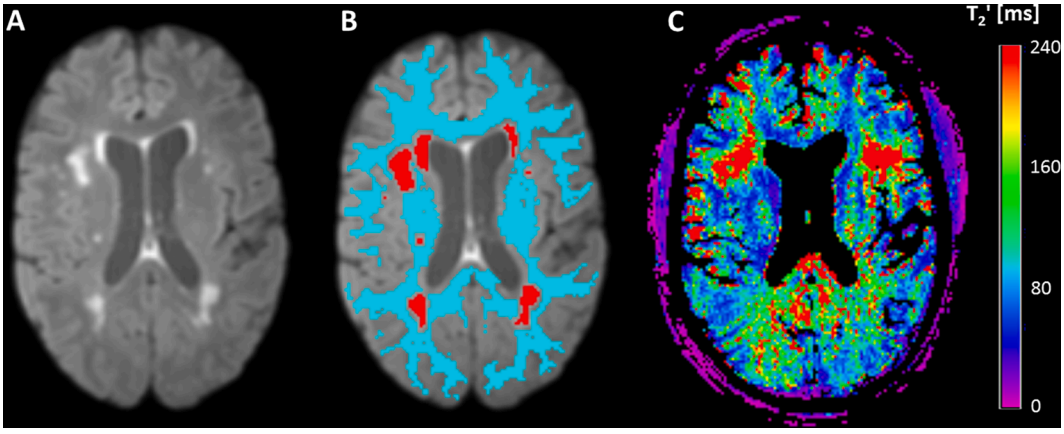

Fig. 2. Illustration of WMH and tissue segmentation in a representative SVD patient. A: brain-extracted FLAIR image; B: brain-extracted FLAIR image with overlaid WMH segmentation (read regions) and WM mask (light blue area); C: coregistered T_2' map. WMH and WM masks were used to extract mean values of T_2' for the respective compartments from the coregistered T_2' parameter map. Note that voxels reflecting CSF were subtracted from the T_2' map before quantitative analysis to minimize partial volume effects. ms: milliseconds.

considered statistically significant.

3. Results

3.1. Demographic characteristics, structural/diffusion imaging and cognitive performance

SVD patients and control subjects did not differ significantly in terms of age (p = 0.527) and sex (p = 0.409). Patients showed significantly impaired global cognitive performance ($p < 0.001$) and impaired global executive functioning ($p = 0.029$). Also in the separate analysis of the 'plus'-subtests, SVD patients exhibited significantly compromised executive function compared to healthy control subjects (z-score TMT-B: -0.52 ± 1.24 vs. 0.52 ± 1.32, $p = 0.013$; z-score 'S-words': -0.43 ± 1.40 vs. 0.63 ± 1.07, $p = 0.017$). With regard to psychomotor speed, no significant group difference could be found (z-score TMT-A: -0.62 ± 1.21 vs. −0.41 ± 1.50, $p = 0.596$).

There was no difference between SVD patient and control subjects regarding the NBV ($p = 0.782$). FA showed a significant decrease across the entire WM and the NAWM of patients compared to control subjects (whole WM: 0.380 ± 0.059 vs 0.436 ± 0.026, $p < 0.001$; NAWM: 0.380 ± 0.061 vs. 0.436 ± 0.025, $p < 0.001$). MD averaged across the entire WM as well as the NAWM was significantly increased in patients compared to controls (whole WM: 0.9563 ± 0.3186 $10^{-3}mm^2s^{-1}$ vs. 0.8178 ± 0.0534 $10^{-3}mm^2s^{-1}$, $p < 0.001$; NAWM: 0.9356 ± 0.3264 $10^{-3}mm^2s^{-1}$ vs. 0.8056 ± 0.0470 $10^{-3}mm^2s^{-1}$, $p = 0.003$).

Demographic baseline characteristics, structural and diffusion imaging parameters as well cognitive performance of SVD patients and healthy control subjects are summarized in Table 1.

3.2. Quantitative T_2' values in the cerebral (NA)WM and within WMH

Quantitative T_2' values averaged across the entire WM and in the NAWM were significantly increased in SVD patients compared to control subjects (149.51 ± 16.94 ms vs. 138.19 ± 12.66 ms, $p = 0.024$ and 147.45 ± 18.14 ms vs. 137.99 ± 12.19 ms, $p = 0.034$; Fig. 3A and B). In the group of SVD patients, T_2' values extracted from the WMH were significantly higher compared to T_2' in the surrounding NAWM ($p < 0.001$, Fig. 3C). A positive correlation between T_2' values averaged across the whole WM as well as within WMH and the normalized lesion volume (to the ICV) was observed (whole WM: ρ=0.441, $p = 0.006$; WMH: ρ=0.564, $p < 0.001$), indicating that higher lesion burden is associated with increased T_2' values (Fig. 4A and B).

Table 1
Demographic baseline characteristics, structural and diffusion imaging parameters and cognitive parameters of SVD patients and control subjects (mean ± SD).

	SVD patients ($n = 32$)	Control subjects ($n = 17$)	p-value
Mean age (years)	70.0 ± 10.2	71.8 ± 7.5	0.527
Female (n (%))	13 (40.6%)	9 (52.9%)	0.409
NBV (cm^3)	1418 ± 68.69	1426 ± 95.44	0.782
WMH volume (cm^3)	25.80 ± 18.76	5.69 ± 5.48	< 0.001
Lacunes (n)	1.06 ± 1.41	0.25 ± 0.77	0.019
Microbleeds (n)	1.06 ± 1.75	0.13 ± 0.34	0.059
FA NAWM	0.380 ± 0.061	0.436 ± 0.025	< 0.001
MD NAWM ($10^{-3}mm^2s^{-1}$)	0.9356 ± 0.3264	0.8056 ± 0.0470	0.003
TMT-A (z-score)	-0.62 ± 1.21	-0.41 ± 1.50	0.596
TMT-B (z-score)	-0.52 ± 1.24	0.52 ± 1.32	0.013
S-Words (z-score)	-0.43 ± 1.40	0.63 ± 1.07	0.017
Global cognitive compound (averaged z-scores)*	-0.67 ± 0.83	0.21 ± 0.60	< 0.001
Executive function compound (averaged z-scores)**	-0.50 ± 1.1	0.25 ± 0.93	0.029

NBV: normalized brain volume; WMH: white matter hyperintensity; FA: fractional anisotropy; MD: mean diffusivity; NAWM: normal-appearing white matter; TMT: trail making test.
* averaged z-scores of the CERAD subtests comprised in the Chandler Score.
** averaged z-scores of the 'plus'-subtests.

3.3. Relationship between quantitative T_2' and intracellular energy metabolism

The pH_i averaged across the volumes-of-interest of both hemispheres was numerically increased in SVD patients compared to control subjects, but the difference was not statistically significant (7.0301 ± 0.04131 vs. 7.0269 ± 0.01538, $p = 0.756$). Furthermore, no significant differences were found between the groups for the ratio PCr/Pi ($p = 0.235$) and the ratio ATP/Pi ($p = 0.423$). PH_i across the entire cohort of subjects showed a significant positive correlation with the averaged T_2' values obtained from the entire segmented WM (ρ = 0.299, $p = 0.044$ (Fig. 4C)) as well as with T_2' values extracted from the WMH (ρ = 0.327, $p = 0.029$ (Fig. 4D)), while no significant associations between T_2' and the ratios PCr/Pi and ATP/Pi were found (p-values ≥ 0.305).

3.4. Relationship between T_2'/pH_i and vascular pulsatility

In the group of SVD patients, quantitative T_2' values extracted from the entire WM as well as from the WMH showed a significant positive correlation with the ICA-PI (entire WM: ρ=0.596, $p = 0.001$ (Fig. 5A); WMH: ρ = 0.475, $p = 0.014$). Furthermore, a significant positive correlation between pH_i and the ICA-PI was observed (ρ = 0.452, $p = 0.016$ (Fig. 5B)).

4. Discussion

In this exploratory and pathophysiological study, ^{31}P MRS and quantitative T_2'-mapping were used to investigate alterations of the tissue oxygen metabolism and pH_i in patients with SVD. The present cohort of SVD patients exhibited significantly compromised WM integrity beyond the visible WMH according to commonly used DTI measures, as well as cognitive impairment compared to healthy controls (Table 1). Global WM T_2' values were significantly increased (Fig. 3A and B) in SVD patients compared to control subjects and prolongation of T_2' was more pronounced within WMH as compared to the surrounding NAWM (Fig. 3B). Furthermore, T_2' values increased with increasing WMH volume (Fig. 4A and B) as a conventional imaging marker of SVD disease severity. T_2' correlated positively with pH_i, suggesting a close coupling between changes of tissue oxygen metabolism and intracellular energy metabolism in SVD (Fig. 4C and D). Both parameters showed significant positive associations with the vascular pulsatility measured in the distal ICA (Fig. 5A and B).

T_2' represents a surrogate marker of the cerebral OEF since it sensitive to locally increased concentrations of deoxygenated hemoglobin in the cerebral capillaries and veins, which lead to a shortening of T_2' [29,31,33]. Our results demonstrated increased T_2' values in SVD patients compared to control subjects (Fig. 3A, B), which indicate a shift towards elevated concentrations of oxygenated hemoglobin [31] and consequently suggest decreased cerebral OEF in the SVD patient group. Although it is still unclear whether this must be interpreted as one of the causes or rather a consequence of this condition [18], SVD is usually associated with reduced CBF [52]. In general, one would assume that in order to preserve the $CMRO_2$, decreased CBF should lead to an OEF increase under ischemic conditions [15,18]. In fact, based on positron emission tomography (PET) measurements, elevated OEF at decreased CBF in patients with SVD has been reported [53,54]. However, although OEF alterations in SVD have been repeatedly demonstrated, the

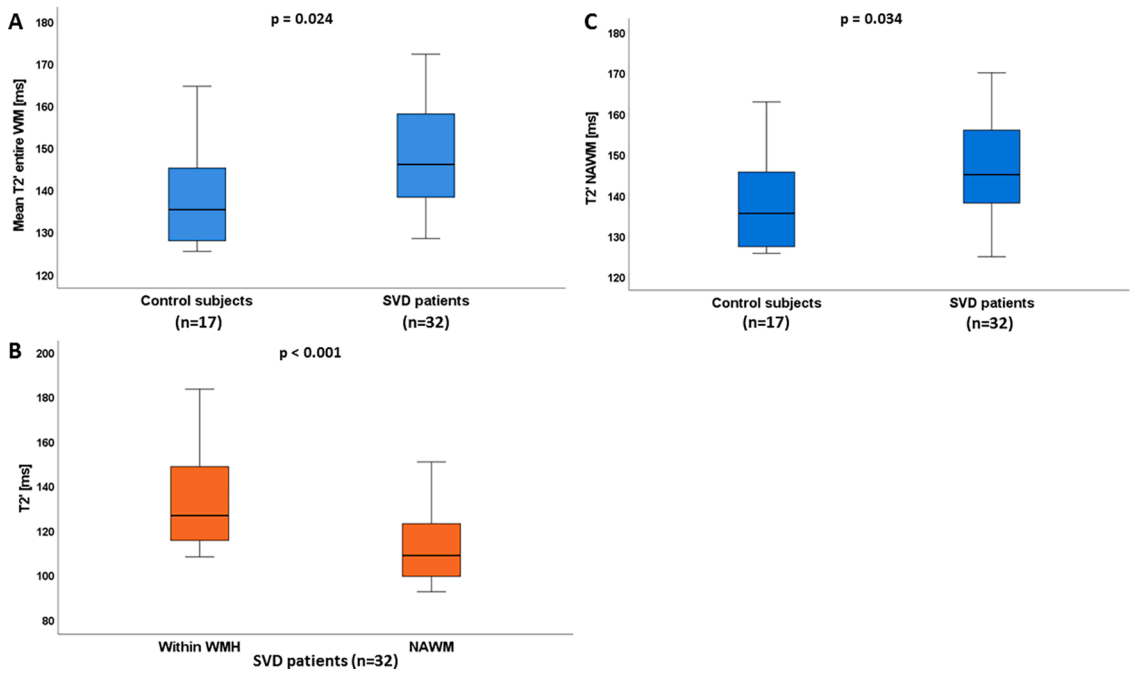

Fig. 3. Boxplots illustrating quantitative T_2' values averaged across the entire (A) and the normal-appearing white matter (B) for SVD patients and control subjects as well as T_2' values within the WMH and the surrounding NAWM for the group of SVD patients (C). SVD patients showed significantly increased T_2' values across the entire segmented WM and the NAWM compared to control subjects and increase of T_2' was more pronounced within the WMH as compared to the surrounding NAWM. ms: milliseconds; WM: white matter; SVD: cerebral small vessel disease; NAWM: normal-appearing white matter; WMH: white matter hyperintensities.

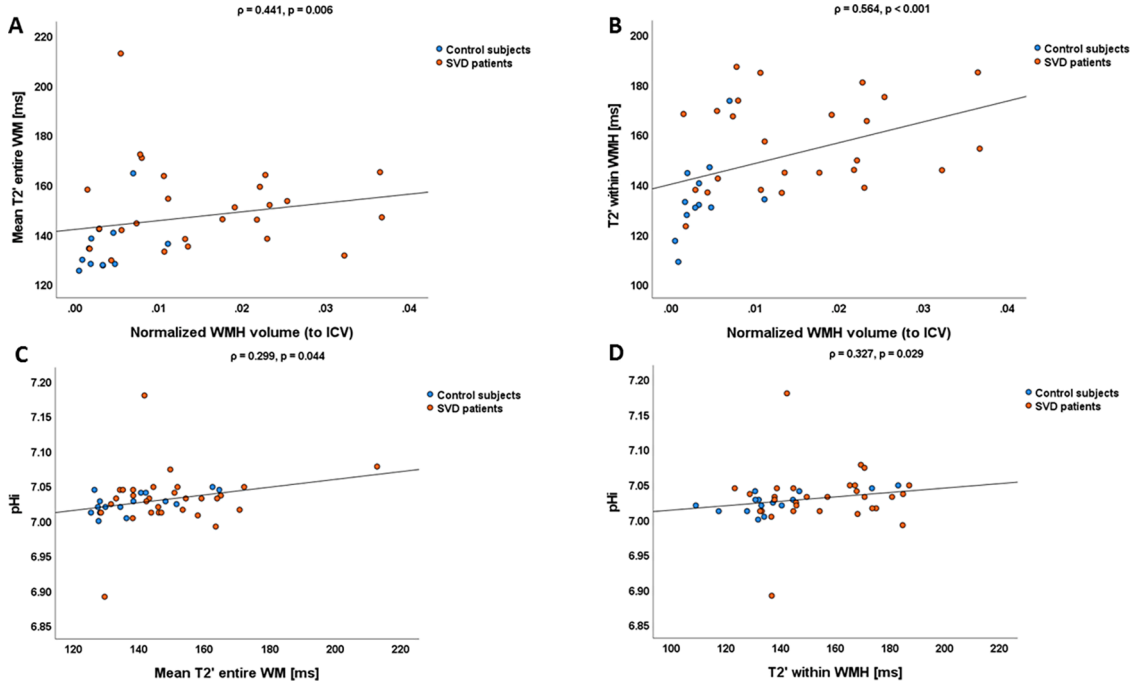

Fig. 4. Scatterplots illustrating the positive correlation between the normalized lesion volume (to the ICV) and T_2' values averaged across the entire WM (A) and within the WMH (B). C and D: Scatterplots illustrating the relationship of pH_i with T_2' values extracted from the entire WM and from the WMH. A line of best fit for the linear relationship between the two variables is shown in each graph. ICV: intracranial volume, ms: milliseconds, WM: white matter, WMH: white matter hyperintensities; pH_i: intracellular pH.

available data in the literature are controversial with regard to the direction of the OEF change since several studies also reported a decrease of the cerebral OEF in SVD [55,56]. One possible explanation for these discrepancies might be the heterogeneity of pathomechanisms leading to the development of WMH and microstructural impairment of the surrounding NAWM, which may affect the tissue oxygen extraction capacity differently or to varying degrees. Apart from disturbed vascular autoregulation, thickening of the vascular wall and increased BBB leakage with enlargement of the extracellular space as well-described features of vascular and microstructural impairment in SVD [20,21,42,

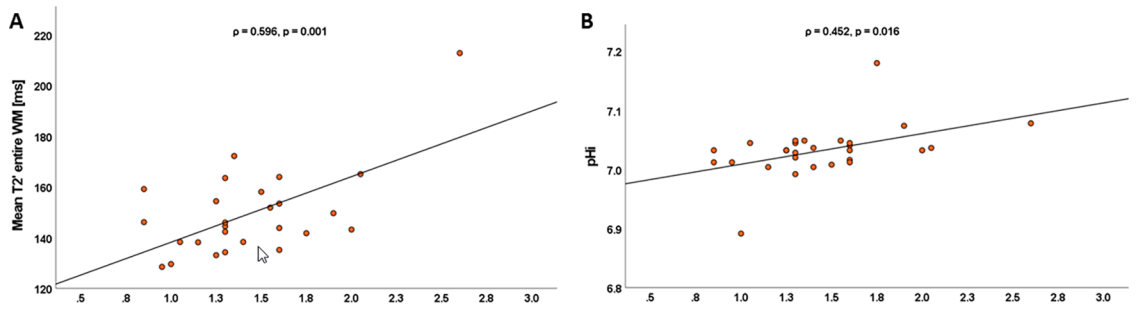

Fig. 5. Scatterplots illustrating the relationship of T_2' values extracted from the entire WM (A) and pH_i (B) with the ICA-PI in the group of SVD patients. A line of best fit for the linear relationship between the two variables is shown in each graph. ms: milliseconds; WM: white matter; ICA-PI: internal carotid artery pulsatility index; pH_i: intracellular pH.

57], capillary dysfunction has been recently suggested as a key pathomechanism actually limiting the cerebral oxygen extraction ability [57]. Since oxygen diffuses passively along the concentration gradient between the capillary blood and the surrounding interstitium/brain tissue, capillary flow patterns have a major impact on the effectiveness of oxygen extraction [18,57]. Capillary dysfunction in the context of cerebral hypoperfusion is defined as the inability of capillary blood flows to homogenize in situations with relatively increased CBF, i.e. upon neuronal activation [57]. Risk factors for SVD such as arterial hypertension and diabetes can compromise capillary flow patterns via pathomechanisms like damage of pericytes, thickening of basal membranes and glycocalyx degradation [57]. Those altered capillary flow patterns characterized by less inhomogeneous blood flow result in a faster transit of the oxygenated blood across the capillary bed, thereby limiting the maximum amount of extractable oxygen and thus impairing the oxygen extraction efficiency [18,56–58]. Initially, this might be compensated by an increase of the CBF, but later on the capillary transit time has to be slowed down through a decrease of the CBF in an attempt to avoid a further drop of the OEF [18]. On the whole, those alterations ultimately lead to a reduction of the $CMRO_2$. According to those pathophysiological considerations, one might assume that our patient collective mainly comprised subjects with capillary dysfunction as the predominant pathomechanism leading to microstructural tissue damage and the development of WMH in this cohort. Apart from the pathomechanistic phenotype underlying the SVD-related ischemic tissue damage, the heterogeneity of oxygen exchange alterations in SVD might also be related to disease severity [55]. Several PET-based studies found reduced CBF and oxygen metabolism in patients with vascular dementia while cognitively unimpaired patients with WMH showed a less decreased CBF, normal oxygen metabolism and even increased OEF [53–56]. Apart from the conclusion that cognitive function in SVD is determined by oxygen metabolism rather than by WMH volume [55], these findings may lead to the assumption that a clinically relevant disease stage is characterized by reduced oxygen metabolism, whereas in earlier subclinical stages a compensatory OEF increase still succeeds. In our study, SVD patients were not evaluated regarding the fulfillment of the criteria for vascular dementia, since this was not an inclusion criterion. Still, SVD patients showed significantly impaired cognitive performance compared to control subjects (Table 1), indicating a clinically relevant stage of the disease. According to the existing literature, the finding of a reduced OEF (reflected by increased T_2') could be well-explained by the fact that our patient group consisted of cognitively impaired subjects instead of asymptomatic elderly subjects with WMH, since cognitive impairment in SVD is associated with compromised oxygen metabolism [53–55].

For pH_i values, no significant difference between SVD patients and healthy control subjects could be detected. Nonetheless, we found a significant relationship between T_2' and pH_i as higher T_2' values - obtained both from the WMH and the entire segmented WM - were significantly associated with increased and thus more alkaline pH_i (Fig. 4C, D). This association suggests a coupling between compromised oxygen metabolism and changes of intracellular energy metabolism reflected by an increasing pH_i in SVD. The question arises which mechanisms in general contribute to the development of an elevated pH_i and how they are related to different pathophysiological aspects in the context of SVD. First of all, the finding of an increased tissue pH in SVD patients is consistent with previous data on subacute and chronic cerebral ischemia, which demonstrated a shift towards alkalosis after an initial period of tissue acidosis [23–26]. Especially ischemic cell necrosis with immigration of inflammatory cells and glial cell proliferation as well as the formation of intracellular edema with alignment of the intracellular and extracellular bicarbonate concentrations have been discussed as underlying pathomechanisms [24,26]. Another possible explanation for an increase of pH_i in chronic cerebral ischemia is an adaptation of brain buffering mechanisms due to initial lactic acidosis, including the upregulation of the Na^+/H^+-antiporter [24] in still viable tissue due to growth factor stimulation and Na^+-influx into the cells. One study reported an association of alkalotic pH with reduced oxygen fraction in subacute cerebral ischemia. This finding was interpreted as a sign of “luxury” perfusion or metabolic paralysis in functionally and structurally impaired ischemic tissue in subacute stroke after (partial) restoration of perfusion [59]. Gliotic tissue conversion as well as inflammatory cell migration have also been described in SVD [60–62], while the tissue edema in SVD - apart from (sub)acute lacunar infarcts - is usually restricted to the extracellular space [20,21]. Since a special isoform of the Na^+/H^+-antiporter (Na^+/H^+-exchanger 1) is induced under hypoxic conditions [63,64] and (relative) cellular hypoxia must be assumed due to impairment of the cerebral oxygen extraction [18,56,58], this ion transporter might play a role with regard to the increasing intracellular alkalosis at increasing T_2' in SVD. Given the significant positive correlation between T_2' values and pH_i, another important mechanism possibly explaining the shift towards more alkaline pH_i values is that an alkaline pH_i leads to an augmentation of the glycolysis rate through an acceleration of key enzymatic reactions and increased enzymatic activity [28]. In this sense, pH_i is the link between impaired oxygen supply, caused by SVD-related pathological alterations of the cerebral vasculature and brain parenchyma, and adaptations of the intracellular energy metabolism. Consequently, the positive relationship between T_2' values and pH_i might reflect the impaired oxygen extraction leading to reduced cellular oxidative phosphorylation, which is compensated by an augmented glycolysis rate [28]. A coupling between glycolysis and oxidative phosphorylation exists also under physiological conditions via the Krebs cycle, but this might be amplified under the condition of cerebral hypoperfusion, respectively reduced oxygen supply, which is reflected by the significant positive relationship between T_2' and pH_i. As we found no significant association between T_2' and the ratios PCr/Pi and ATP/Pi, this cellular adaptation mechanism seems to be sufficient to maintain overall normal intracellular concentrations of the high-energy metabolites PCr and ATP. In case of decreasing

intracellular concentrations of energy-rich metabolites as a consequence of impaired cellular OEF, a significant negative of relationship of T_2' with the ratios PCr/Pi and ATP/Pi would be expected. Both T_2' values and pH_i showed significant positive correlations with the pulsatility measured in the distal ICA (Fig. 5A, B), suggesting more pronounced impairment of the OEF and increasing intracellular alkalosis at increased vascular stiffness and compromised cerebral autoregulation [65,66]. Since the latter may affect the cerebral microcirculation and consequently also the oxygen and energy metabolism, and an elevated PI is associated with both disease severity and progression of SVD [66,67], those findings are in line with the previous pathophysiological considerations.

4.1. Limitations

This study has several limitations. First of all, the sample size is relatively small, which might affect in particular the detectability of significant differences in pH_i since the numerical differences between SVD patients and healthy control subjects are generally small for this parameter. However, it should be considered that due to the relatively long acquisition time necessary for combined quantitative MRI, DTI and MRS, it is difficult to obtain the data presented in this study in an elderly patient collective with clinically relevant cerebrovascular disease - especially because additional comprehensive cognitive testing was performed. Furthermore, since this is not a longitudinal study, we cannot comment on potential changes of T_2' and pH_i over time and the dynamics of those in SVD, which may depend on the disease stage. Future studies should use larger sample sizes and a longitudinal design along with systematic analyses of other clinical SVD features going beyond cognitive decline, such as gait impairment. Although 3D ^{31}P MRS data were acquired and thus the entire brain was covered to perform metabolite measurements, we deal with a poor point spread function in ^{31}P MRS, which means that there is significant signal from the region close to the targeted voxel. This is a potential limitation when restricted lesions or areas are targeted as regions-of-interest. In addition, ^{31}P harbors some important technical limitations including a low signal-to-noise ratio and poor spatial resolution, making it prone to partial volume effects and potentially affecting the obtained metabolite and parameter measurements. Finally, some of the mechanisms described in our interpretations have not yet been entirely elucidated. Consequently, although they are plausible from the mechanistic and pathophysiological point of view, some of our causative explanations are still subject to uncertainty and should be generalized with caution. Our findings require confirmation in larger cohorts with even more comprehensive imaging protocols.

5. Conclusions

In conclusion, using combined ^{31}P MRS and oxygenation-sensitive quantitative T_2'-mapping, this exploratory and pathophysiological study demonstrates impaired cerebral oxygen extraction and compensatory mechanisms through the adjustment of intracellular energy metabolism by an elevated pH_i in SVD. Our findings are plausible from the pathophysiological point of view and point towards a tight coupling between changes of cerebral oxygen extraction and other changes of intracellular energy metabolism. Our findings provide important insights into the pathophysiology of SVD with regard to alterations of the cellular energy metabolism presumably related to an impairment of the cerebral microcirculation and the microstructural tissue integrity.

Funding

This work was supported by the Else-Kröner-Fresenius-Stiftung (research grant to RMG and AS) and by the Clinician Scientist program of the Goethe University Frankfurt/Faculty of Medicine (research grant to AS).

Declaration of Competing Interest

The authors declare that there are no conflicts of interest related to this article.

Acknowledgments

None.

References

[1] L. Pantoni, Cerebral small vessel disease: from pathogenesis and clinical characteristics to therapeutic challenges, Lancet Neurol. 9 (2010) 689–701, https://doi.org/10.1016/S1474-4422(10)70104-6. PMID: 20610345.
[2] N.D. Prins, E.J. van Dijk, H.T. Den, S.E. Vermeer, J. Jolles, P.J. Koudstaal, et al., Cerebral small-vessel disease and decline in information processing speed, executive function and memory, Brain 128 (2005) 2034–2041, https://doi.org/10.1093/brain/awh553. Epub 2005/06/09PMID: 15947059.
[3] N.D. Prins, P. Scheltens, White matter hyperintensities, cognitive impairment and dementia: an update, Nat. Rev. Neurol. 11 (2015) 157–165, https://doi.org/10.1038/nrneurol.2015.10. Epub 2015/02/17PMID: 25686760.
[4] S. Debette, H.S. Markus, The clinical importance of white matter hyperintensities on brain magnetic resonance imaging: systematic review and meta-analysis, BMJ 341 (2010) c3666, https://doi.org/10.1136/bmj.c3666. Epub 2010/07/26PMID: 20660506.
[5] J.M. Wardlaw, C. Smith, M. Dichgans, Mechanisms of sporadic cerebral small vessel disease: insights from neuroimaging, Lancet Neurol. 12 (2013) 483–497, https://doi.org/10.1016/S1474-4422(13)70060-7. PMID: 23602162.
[6] F. Fazekas, R. Kleinert, H. Offenbacher, R. Schmidt, G. Kleinert, F. Payer, et al., Pathologic correlates of incidental MRI white matter signal hyperintensities, Neurology 43 (1993) 1683–1689, https://doi.org/10.1212/wnl.43.9.1683. PMID: 8414012.
[7] F. Fazekas, R. Schmidt, P. Scheltens, Pathophysiologic mechanisms in the development of age-related white matter changes of the brain, Dement. Geriatr. Cogn. Disord. 9 (1) (1998) 2–5, https://doi.org/10.1159/000051182. SupplPMID: 9716237.
[8] H.S. Markus, D.J. Lythgoe, L. Ostegaard, M. O'Sullivan, S.C. Williams, Reduced cerebral blood flow in white matter in ischaemic leukoaraiosis demonstrated using quantitative exogenous contrast based perfusion MRI, J. Neurol. Neurosurg. Psychiatry 69 (2000) 48–53, https://doi.org/10.1136/jnnp.69.1.48. PMID: 10864603.
[9] R.B. Dalby, S.F. Eskildsen, P. Videbech, J. Frandsen, K. Mouridsen, L. Sørensen, et al., Oxygenation differs among white matter hyperintensities, intersected fiber tracts and unaffected white matter, Brain Commun. 1 (2019) fcz033, https://doi.org/10.1093/braincomms/fcz033. Epub 2019/11/18PMID: 32954272.
[10] M. O'Sullivan, D.J. Lythgoe, A.C. Pereira, P.E. Summers, J.M. Jarosz, S.C. R. Williams, et al., Patterns of cerebral blood flow reduction in patients with ischemic leukoaraiosis, Neurology 59 (2002) 321–326, https://doi.org/10.1212/wnl.59.3.321. PMID: 12177363.
[11] N.O. Promjunyakul, D.L. Lahna, J.A. Kaye, H.H. Dodge, D. Erten-Lyons, W. D. Rooney, et al., Comparison of cerebral blood flow and structural penumbras in relation to white matter hyperintensities: a multi-modal magnetic resonance imaging study, J. Cereb. Blood Flow Metab. 36 (2016) 1528–1536, https://doi.org/10.1177/0271678X16651268. Epub 2016/06/07PMID: 27270266.
[12] P. Maillard, E. Fletcher, D. Harvey, O. Carmichael, B. Reed, D. Mungas, et al., White matter hyperintensity penumbra, Stroke 42 (2011) 1917–1922, https://doi.org/10.1161/STROKEAHA.110.609768. Epub 2011/06/02PMID: 21636811.
[13] A. Seiler, A. Jurcoane, J. Magerkurth, M. Wagner, E. Hattingen, R. Deichmann, et al., T2′ imaging within perfusion-restricted tissue in high-grade occlusive carotid disease, Stroke 43 (2012) 1831–1836, https://doi.org/10.1161/STROKEAHA.111.646109. Epub 2012/05/08PMID: 22569938.
[14] C.P. Derdeyn, T.O. Videen, K.D. Yundt, S.M. Fritsch, D.A. Carpenter, R.L. Grubb, et al., Variability of cerebral blood volume and oxygen extraction: stages of cerebral haemodynamic impairment revisited, Brain 125 (2002) 595–607, https://doi.org/10.1093/brain/awf047. PMID: 11872616.
[15] C.P. Derdeyn, Hemodynamics and oxygen extraction in chronic large artery steno-occlusive disease: clinical applications for predicting stroke risk, J. Cereb. Blood Flow Metab. 38 (2018) 1584–1597, https://doi.org/10.1177/0271678X17732884. Epub 2017/09/19PMID: 28925313.
[16] A. Seiler, R. Deichmann, W. Pfeilschifter, E. Hattingen, O.C. Singer, M. Wagner, T2-imaging to assess cerebral oxygen extraction fraction in carotid occlusive disease: influence of cerebral autoregulation and cerebral blood volume, PLoS One 11 (2016), e0161408, https://doi.org/10.1371/journal.pone.0161408. Epub 2016/08/25PMID: 27560515.
[17] L. Østergaard, T.S. Engedal, F. Moreton, M.B. Hansen, J.M. Wardlaw, T. Dalkara, et al., Cerebral small vessel disease: capillary pathways to stroke and cognitive decline, J. Cereb. Blood Flow Metab. 36 (2016) 302–325, https://doi.org/10.1177/0271678X15606723. Epub 2015/10/14PMID: 26661176.
[18] S.N. Jespersen, L. Østergaard, The roles of cerebral blood flow, capillary transit time heterogeneity, and oxygen tension in brain oxygenation and metabolism, J. Cereb. Blood Flow Metab. 32 (2012) 264–277, https://doi.org/10.1038/jcbfm.2011.153. Epub 2011/11/02PMID: 22044867.

[19] G.W. Blair, F.N. Doubal, M.J. Thrippleton, I. Marshall, J.M. Wardlaw, Magnetic resonance imaging for assessment of cerebrovascular reactivity in cerebral small vessel disease: a systematic review, J. Cereb. Blood Flow Metab. 36 (2016) 833–841, https://doi.org/10.1177/0271678X16631756. Epub 2016/02/16PMID: 26884471.

[20] M. Duering, S. Finsterwalder, E. Baykara, A.M. Tuladhar, B. Gesierich, M. J. Konieczny, et al., Free water determines diffusion alterations and clinical status in cerebral small vessel disease, Alzheimers Dement. 14 (2018) 764–774, https://doi.org/10.1016/j.jalz.2017.12.007. Epub 2018/02/16PMID: 29406155.

[21] M.J. Thrippleton, W.H. Backes, S. Sourbron, M. Ingrisch, M.J. van Osch, M. Dichgans, et al., Quantifying blood-brain barrier leakage in small vessel disease: review and consensus recommendations, Alzheimer Dement. 15 (2019) 840–858, https://doi.org/10.1016/j.jalz.2019.01.013. Epub 4/25/2019PMID: 31031101.

[22] A. Henning, Proton and multinuclear magnetic resonance spectroscopy in the human brain at ultra-high field strength: a review, NeuroImage 168 (2018) 181–198, https://doi.org/10.1016/j.neuroimage.2017.07.017. Epub 2017/07/13PMID: 28712992.

[23] J.P. Zöllner, E. Hattingen, O.C. Singer, Pilatus U. Changes of pH and energy state in subacute human ischemia assessed by multinuclear magnetic resonance spectroscopy, Stroke 46 (2015) 441–446, https://doi.org/10.1161/STROKEAHA.114.007896. Epub 2014/12/11PMID: 25503553.

[24] J.W. Hugg, J.H. Duijn, G.B. Matson, A.A. Maudsley, J.S. Tsuruda, D.F. Gelinas, et al., Elevated lactate and alkalosis in chronic human brain infarction observed by 1H and 31P MR spectroscopic imaging, J. Cereb. Blood Flow Metab. 12 (1992) 734–744, https://doi.org/10.1038/jcbfm.1992.104. PMID: 1506441.

[25] T. Nakada, K. Houkin, K. Hida, I.L. Kwee, Rebound alkalosis and persistent lactate: multinuclear (1H, 13C, 31P) NMR spectroscopic studies in rats, Magn. Reson. Med. 18 (1991) 9–14, https://doi.org/10.1002/mrm.1910180103. PMID: 2062245.

[26] S.R. Levine, J.A. Helpern, K.M. Welch, A.M.V. Linde, K.L. Sawaya, E.E. Brown, et al., Human focal cerebral ischemia: evaluation of brain pH and energy metabolism with P-31 NMR spectroscopy, Radiology 185 (1992) 537–544, https://doi.org/10.1148/radiology.185.2.1410369. PMID: 1410369.

[27] A. Seiler, S. Kammerer, A. Gühl, J.R. Schüre, R. Deichmann, U. Nöth, et al., Revascularization of high-grade carotid stenosis restores global cerebral energy metabolism, Stroke 50 (2019) 1742–1750, https://doi.org/10.1161/STROKEAHA.118.023559. Epub 2019/06/05PMID: 31164069.

[28] A. Syrota, Y. Samson, C. Boullais, P. Wajnberg, C. Loc'h, C. Crouzel, et al., Tomographic mapping of brain intracellular pH and extracellular water space in stroke patients, J. Cereb. Blood Flow Metab. 5 (1985) 358–368, https://doi.org/10.1038/jcbfm.1985.50. PMID: 3875620.

[29] B.S. Geisler, F. Brandhoff, J. Fiehler, C. Saager, O. Speck, J. Röther, et al., Blood-oxygen-level-dependent MRI allows metabolic description of tissue at risk in acute stroke patients, Stroke 37 (2006) 1778–1784, https://doi.org/10.1161/01.STR.0000226738.97426.6f. Epub 2006/06/01PMID: 16741186.

[30] H. Tamura, J. Hatazawa, H. Toyoshima, E. Shimosegawa, T. Okudera, Detection of deoxygenation-related signal change in acute ischemic stroke patients by T2*-weighted magnetic resonance imaging, Stroke 33 (2002) 967–971, https://doi.org/10.1161/01.STR.0000013672.70986.E2. PMID: 11935045.

[31] H. An, W. Lin, Quantitative measurements of cerebral blood oxygen saturation using magnetic resonance imaging, J. Cereb. Blood Flow Metab. 20 (2000) 1225–1236, https://doi.org/10.1097/00004647-200008000-00008. PMID: 10950383.

[32] K.R. Thulborn, J.C. Waterton, P.M. Matthews, G.K. Radda, Oxygenation dependence of the transverse relaxation time of water protons in whole blood at high field, Biochim. Biophys. Acta 714 (1982) 265–270, https://doi.org/10.1016/0304-4165(82)90333-6. PMID: 6275909.

[33] U. Jensen-Kondering, J.C. Baron, Oxygen imaging by MRI: can blood oxygen level-dependent imaging depict the ischemic penumbra, Stroke 43 (2012) 2264–2269, https://doi.org/10.1161/STROKEAHA.111.632455. Epub 2012/05/15PMID: 22588263.

[34] A. Brandhofe, C. Stratmann, J.R. Schüre, U. Pilatus, E. Hattingen, R. Deichmann, et al., T2 relaxation time of the normal-appearing white matter is related to the cognitive status in cerebral small vessel disease, J. Cereb. Blood Flow Metab. 41 (2021) 1767–1777, https://doi.org/10.1177/0271678X20972511. Epub 2020/12/16PMID: 33327818.

[35] V.A. van den Boogaart, S. van Huffel, Improved method for accurate and efficient quantification of MRS data with use of prior knowledge, J. Magn. Reson. 129 (1997) 35–43, https://doi.org/10.1006/jmre.1997.1244. PMID: 9405214.

[36] O.A. Petroff, J.W. Prichard, K.L. Behar, J.R. Alger, H.J.A. Den, R.G. Shulman, Cerebral intracellular pH by 31P nuclear magnetic resonance spectroscopy, Neurology (1985) 35, https://doi.org/10.1212/wnl.35.6.781. PMID: 4000479.

[37] D.W. Zochodne, R.T. Thompson, A.A. Driedger, M.J. Strong, D. Gravelle, C. F. Bolton, Metabolic changes in human muscle denervation: topical 31P NMR spectroscopy studies, Magn. Reson. Med. 7 (1988) 373–383, https://doi.org/10.1002/mrm.1910070402. PMID: 3173055.

[38] S.M. Smith, Fast robust automated brain extraction, Hum. Brain Mapp. 17 (2002) 143–155, https://doi.org/10.1002/hbm.10062. PMID: 12391568.

[39] U. Nöth, S. Volz, E. Hattingen, R. Deichmann, An improved method for retrospective motion correction in quantitative T2* mapping, NeuroImage 92 (2014) 106–119, https://doi.org/10.1016/j.neuroimage.2014.01.050. Epub 2014/02/04PMID: 24508652.

[40] A.M. Tuladhar, A.G.W. van Norden, L.K.F. De, M.P. Zwiers, E.J. van Dijk, D. G. Norris, et al., White matter integrity in small vessel disease is related to cognition, NeuroImage Clin. 7 (2015) 518–524, https://doi.org/10.1016/j.nicl.2015.02.003. Epub 2015/02/16PMID: 25737960.

[41] I.W.M. van Uden, A.M. Tuladhar, L.K.F. De, A.G.W. van Norden, D.G. Norris, E. J. van Dijk, et al., White matter integrity and depressive symptoms in cerebral small vessel disease: the RUN DMC study, Am. J. Geriatr. Psychiatry 23 (2015) 525–535, https://doi.org/10.1016/j.jagp.2014.07.002. Epub 2014/07/19PMID: 25151438.

[42] J.M. Wardlaw, E.E. Smith, G.J. Biessels, C. Cordonnier, F. Fazekas, R. Frayne, et al., Neuroimaging standards for research into small vessel disease and its contribution to ageing and neurodegeneration, Lancet Neurol. 12 (2013) 822–838, https://doi.org/10.1016/S1474-4422(13)70124-8.

[43] M. Jenkinson, Improved optimization for the robust and accurate linear registration and motion correction of brain images, NeuroImage 17 (2002) 825–841, https://doi.org/10.1016/s1053-8119(02)91132-8. PMID: 12377157.

[44] S.M. Smith, M. Jenkinson, M.W. Woolrich, C.F. Beckmann, T.E.J. Behrens, H. Johansen-Berg, et al., Advances in functional and structural MR image analysis and implementation as FSL, NeuroImage 23 (1) (2004) S208–S219, https://doi.org/10.1016/j.neuroimage.2004.07.051. SupplPMID: 15501092.

[45] S.M. Smith, Y. Zhang, M. Jenkinson, J. Chen, P.M. Matthews, A. Federico, et al., Accurate, robust, and automated longitudinal and cross-sectional brain change analysis, NeuroImage 17 (2002) 479–489, https://doi.org/10.1006/nimg.2002.1040. PMID: 12482100.

[46] J.C. Morris, R.C. Mohs, H. Rogers, G. Fillenbaum, A. Heyman, Consortium to establish a registry for Alzheimer's disease (CERAD) clinical and neuropsychological assessment of Alzheimer's disease, Psychopharmacol. Bull. 24 (1988) 641–652.

[47] N.S. Schmid, M.M. Ehrensperger, M. Berres, I.R. Beck, A.U. Monsch, The extension of the German CERAD neuropsychological assessment battery with tests assessing subcortical, executive and frontal functions improves accuracy in dementia diagnosis, Dement. Geriatr. Cogn. Dis. Extra 4 (2014) 322–334, https://doi.org/10.1159/000357774. Epub 2014/08/27PMID: 25298776.

[48] M. Berres, A.U. Monsch, F. Bernasconi, B. Thalmann, H.B. Stähelin, Normal ranges of neuropsychological tests for the diagnosis of Alzheimer's disease, Stud. Health Technol. Inform. 77 (2000) 195–199.

[49] D.W. Desmond, The neuropsychology of vascular cognitive impairment: is there a specific cognitive deficit, J. Neurol. Sci. 226 (2004) 3–7, https://doi.org/10.1016/j.jns.2004.09.002. PMID: 15537510.

[50] B.R. Reed, D.M. Mungas, J.H. Kramer, W. Ellis, H.V. Vinters, C. Zarow, et al., Profiles of neuropsychological impairment in autopsy-defined Alzheimer's disease and cerebrovascular disease, Brain 130 (2007) 731–739, https://doi.org/10.1093/brain/awl385. Epub 2007/01/31PMID: 17267522.

[51] M.J. Chandler, L.H. Lacritz, L.S. Hynan, H.D. Barnard, G. Allen, M. Deschner, et al., A total score for the CERAD neuropsychological battery, Neurology 65 (2005) 102–106, https://doi.org/10.1212/01.wnl.0000167607.63000.38. PMID: 16009893.

[52] Y. Shi, M.J. Thrippleton, S.D. Makin, I. Marshall, M.I. Geerlings, C.A.J.M. De, et al., Cerebral blood flow in small vessel disease: a systematic review and meta-analysis, J. Cereb. Blood Flow Metab. 36 (2016) 1653–1667, https://doi.org/10.1177/0271678X16662891. Epub 2016/08/05PMID: 27496552.

[53] K. Meguro, J. Hatazawa, T. Yamaguchi, M. Itoh, T. Matsuzawa, S. Ono, et al., Cerebral circulation and oxygen metabolism associated with subclinical periventricular hyperintensity as shown by magnetic resonance imaging, Ann. Neurol. 28 (1990) 378–383, https://doi.org/10.1002/ana.410280313. PMID: 2241119.

[54] J. Hatazawa, E. Shimosegawa, T. Satoh, H. Toyoshima, T. Okudera, Subcortical hypoperfusion associated with asymptomatic white matter lesions on magnetic resonance imaging, Stroke 28 (1997) 1944–1947, https://doi.org/10.1161/01.str.28.10.1944. PMID: 9341700.

[55] H. Yao, S. Sadoshima, S. Ibayashi, Y. Kuwabara, Y. Ichiya, M. Fujishima, Leukoaraiosis and dementia in hypertensive patients, Stroke 23 (1992) 1673–1677, https://doi.org/10.1161/01.str.23.11.1673. PMID: 1440720.

[56] M.R. Juttukonda, K.A. Stephens, Y.F. Yen, C.M. Howard, J.R. Polimeni, B.R. Rosen, et al., Oxygen extraction efficiency and white matter lesion burden in older adults exhibiting radiological evidence of capillary shunting, J. Cereb. Blood Flow Metab. 42 (2022) 1933–1943, https://doi.org/10.1177/0271678X221105986. Epub 2022/06/08PMID: 35673981.

[57] L. Østergaard, S.N. Jespersen, T. Engedahl, E. Gutiérrez Jiménez, M. Ashkanian, M. B. Hansen, et al., Capillary dysfunction: its detection and causative role in dementias and stroke, Curr. Neurol. Neurosci. Rep. 15 (2015) 37, https://doi.org/10.1007/s11910-015-0557-x. PMID: 25956993.

[58] H. Angleys, L. Østergaard, S.N. Jespersen, The effects of capillary transit time heterogeneity (CTH) on brain oxygenation, J. Cereb. Blood Flow Metab. 35 (2015) 806–817, https://doi.org/10.1038/jcbfm.2014.254. Epub 2015/02/11PMID: 25669911.

[59] A. Syrota, M. Castaing, D. Rougemont, M. Berridge, J.C. Baron, M.G. Bousser, et al., Tissue acid-base balance and oxygen metabolism in human cerebral infarction studied with positron emission tomography, Ann. Neurol. 14 (1983) 419–428, https://doi.org/10.1002/ana.410140405. PMID: 6416140.

[60] R.P.W. Rouhl, J.G.M.C. Damoiseaux, J. Lodder, R. Theunissen, I.L.H. Knottnerus, J. Staals, et al., Vascular inflammation in cerebral small vessel disease, Neurobiol. Aging 33 (2012) 1800–1806, https://doi.org/10.1016/j.neurobiolaging.2011.04.008. Epub 2011/05/23PMID: 21601314.

[61] G.A. Rosenberg, Extracellular matrix inflammation in vascular cognitive impairment and dementia, Clin. Sci. 131 (2017) 425–437, https://doi.org/10.1042/CS20160604 (Lond)PMID: 28265034.

[62] G.A. Rosenberg, Binswanger's disease: biomarkers in the inflammatory form of vascular cognitive impairment and dementia, J. Neurochem. 144 (2018) 634–643, https://doi.org/10.1111/jnc.14218. Epub 2017/11/06PMID: 28902409.

[63] L.A. Shimoda, M. Fallon, S. Pisarcik, J. Wang, G.L. Semenza, HIF-1 regulates hypoxic induction of NHE1 expression and alkalinization of intracellular pH in pulmonary arterial myocytes, Am. J. Physiol. Lung Cell Mol. Physiol. 291 (2006) L941–L949, https://doi.org/10.1152/ajplung.00528.2005. Epub 2006/06/09PMID: 16766575.

[64] P. Cengiz, N. Kleman, K. Uluc, P. Kendigelen, T. Hagemann, E. Akture, et al., Inhibition of Na+/H+ exchanger isoform 1 is neuroprotective in neonatal hypoxic ischemic brain injury, Antioxid. Redox Signal. 14 (2011) 1803–1813, https://doi.org/10.1089/ars.2010.3468. Epub 2010/12/04PMID: 20712402.

[65] G.W. Blair, M.J. Thrippleton, Y. Shi, I. Hamilton, M. Stringer, F. Chappell, et al., Intracranial hemodynamic relationships in patients with cerebral small vessel disease, Neurology 94 (2020) e2258–e2269, https://doi.org/10.1212/WNL.0000000000009483. Epub 2020/05/04PMID: 32366534.

[66] A. Webb, D. Werring, J. Dawson, A. Rothman, A. Lawson, K. Wartolowska, Design of a randomised, double-blind, crossover, placebo-controlled trial of effects of sildenafil on cerebrovascular function in small vessel disease: oxford haemodynamic adaptation to reduce pulsatility trial (OxHARP), Eur. Stroke J. 6 (2021) 283–290, https://doi.org/10.1177/23969873211026698. Epub 2021/06/23PMID: 34746425.

[67] Y. Shi, M.J. Thrippleton, G.W. Blair, D.A. Dickie, I. Marshall, I. Hamilton, et al., Small vessel disease is associated with altered cerebrovascular pulsatility but not resting cerebral blood flow, J. Cereb. Blood Flow Metab. 40 (2020) 85–99, https://doi.org/10.1177/0271678X18803956. Epub 2018/10/08PMID: 30295558.